Available online at www.sciencedirect.com
SCIENCE DIRECT®
International Journal of Heat and Mass Transfer 47 (2004) 2403–2415
International Journal of HEAT and MASS TRANSFER
www.elsevier.com/locate/ijhmt

Nonlinear k–ε–f_μ model and its application to the flow and heat transfer in a channel having one undulant wall

Tae Seon Park [a], Hang Seok Choi [b], Kenjiro Suzuki [c,*]

[a] Rocket Engine Research Development, Korea Aerospace Research Institute, 45 Oun-dong, Yusong-ku, Taejon 305-333, South Korea
[b] Department of Mechanical Engineering, Kyoto University, Kyoto 606-8501, Japan
[c] Department of Machinery and Control Systems, Shibaura Institute of Technology, 307 Fukasaku, Saitama 337-8570, Japan

Received 27 November 2002

Abstract

Turbulent flows and related heat transfer over a fully developed wavy channel is investigated by a turbulence model. The nonlinear k–ε–f_μ model of Park et al. [Int. J. Heat Fluid Flow 24 (2003) 29] is slightly modified and their explicit heat flux model is employed. The Reynolds number is fixed at $Re_b = 6760$ through all wave amplitudes and the wave amplitude is varied in the range $0 \leqslant a/\lambda \leqslant 0.15$. The predicted results for wavy channel are validated by with comparing the DNS data of Maaß and Schumann [Flow Simulation with High Performance Computers, Notes on Numerical Fluid Mechanics 52 (1996) 227]. The model performance is shown to be generally satisfactory. By using k–ε–f_μ model, the enhancement of heat transfer and the characteristics of turbulent flow in wavy wall are investigated. Finally, the effects of wavy amplitude on separated shear layer and its consequent influence on heat transfer are scrutinized.

Keywords: Wavy wall; Nonlinear k–ε–f_μ model; Explicit heat flux model

1. Introduction

Turbulent flows over a wavy wall display peculiar characteristics that are not found in flows over a flat wall. For example, the surface undulation induces the alternating occurrence of favorable and adverse pressure gradients and the periodic changes of streamline curvature. In the case of a deep undulation, recirculating flow region appears near the trough of the wavy wall. These phenomena occurring in wavy wall channels are of great interest in many engineering applications especially, in the enhancement of heat transfer.

In order to understand the effects of waviness of walls on turbulence, many experimental and numerical studies have been carried out. Buckles et al. [1] experimentally identified the three flow regions such as the separated region, an attached boundary layer and free shear layer formed by the separation of the boundary layer. Hudson et al. [3] performed the measurements of the spatial and time variation of velocity components and turbulence quantities. Their work showed that turbulence production in the flow near the wavy surface is different from that in the flow on a flat surface. It is mainly associated with the interactions between the free shear layer and the separated flow region. Maaß and Schumann [4] did a direct numerical simulation (DNS) of turbulent flows over a wavy boundary and compared their results with the measurements by Hudson et al. [3]. They showed the effective friction velocity is about 50% larger at the wavy lower surface than at the flat upper surface mainly because of the additional pressure drag. Cherukat et al. [5] also found by DNS that the velocity bursts originated from the separated flow region remains active over large distance away from the wavy wall. Matsubara et al. [6] showed the heat transfer enhancement in asymmetric wavy surfaces.

On the other hand, several researchers have solved the time-averaged Navier–Stokes equations for the turbulent flow over wavy walls of large amplitude. McLean

* Corresponding author. Tel.: +81-48-687-5155; fax: +81-48-687-5197.
E-mail address: ksuzuki@sic.shibaura-it.ac.jp (K. Suzuki).

0017-9310/$ - see front matter © 2003 Elsevier Ltd. All rights reserved.
doi:10.1016/j.ijheatmasstransfer.2003.10.038

Nomenclature

a	wall wave amplitude
b_{ij}	anisotropy tensor, $\overline{u_iu_j}/2k - \delta_{ij}/3$
C_f	skin friction coefficient, $2\tau_{wall}/\rho U_b^2$
C_p	pressure coefficient, $2P_{wall}/\rho U_b^2$
C_μ, $C_{\varepsilon1}$, $C_{\varepsilon2}$	model constants
D_H	hydraulic diameter, $2H$
f_μ, f_2, f_λ	model functions
H	channel height
k_f	thermal conductivity
Nu	Nusselt number, $Nu = hD_H/k_f = q''_wD_H/k_f(\Theta_w - \Theta_b)$
P	mean pressure
P_k	production of turbulent kinetic energy, $P_k = -\overline{u_iu_j}\partial U_i/\partial x_j$
Pr	Prandtl number, $Pr = \nu/\alpha$
Pr_t	turbulent Prandtl number
P_{wall}	wall pressure
q''_w	wall heat flux
Re_b	Reynolds number, $Re_b = U_bH/\nu$
Re_τ	Reynolds number, $Re_\tau = 0.5u_\tau H/\nu$
R_t	turbulent Reynolds number, $R_t = k^2/\nu\varepsilon$
S_{ij}	strain rate tensor, $S_{ij} = 0.5(U_{i,j} + U_{j,i})$
St	Stanton number, $St = q''_w/(\rho C_pU_b)/(\Theta_w - \Theta_b)$
t	time
u_j	fluctuating velocities
$\overline{u_iu_j}$	Reynolds stress
u_τ	friction velocity
U_b	bulk mean velocity
U_j	mean velocities
W_{ij}	vorticity tensor, $W_{ij} = 0.5(U_{i,j} - U_{j,i})$

Greek symbols

α_t	thermal eddy diffusivity
β_i	coefficients of nonlinear stress–strain relation
γ_i	coefficients of nonlinear heat flux model
λ	wavelength
ν	kinematic molecular viscosity
ν_t	eddy viscosity
ρ	density
τ_{wall}	wall shear stress
θ	fluctuating temperature
θ_τ	friction temperature, $\theta_\tau = q''_w/(\rho C_pu_\tau)$
Θ	mean temperature
Θ^+	nondimensional mean temperature, $\Theta^+ = (\Theta_w - \Theta)/\theta_\tau$
Θ_b	bulk mean temperature
Θ_w	wall temperature

[7] obtained the distribution of wall pressure and shear stress using an algebraic eddy viscosity model. For small-amplitude wavy wall, their predictions agree well with the experimental data. For larger-amplitude wavy wall, appearance of reverse flow region is predicted in the wave trough region. In a two-dimensional wavy channel, Patel et al. [8] explored steady flows with the standard k–ε model employing one-equation near-wall treatment. They described the effects of alternating pressure gradients induced by the periodic change of surface curvatures. The results were judged to capture the overall features including the breakdown of the logarithmic law of the wall in separated flow region. However, as they pointed out, it is needed to develop a more accurate turbulence model.

To analyze the accompanying heat transfer, comprehensive knowledge of flow structure is indispensable. Furthermore, to predict the heat transfer in a wavy channel accurately, reliable flow computations should be preceded. The direct numerical simulation seems to be promising for resolving turbulent motions in detail. However, it requires big computer resources and large CPU time. On the other hand, numerical solutions based on the turbulence model are cost effective in practical applications. Recently, Park et al. [9] developed a nonlinear stress–strain relationship and an explicit algebraic heat flux model (EAHM) on the basis of the linear k–ε–f_μ model of Park and Sung [10]. The nonlinear formulation was derived from the Cayley–Hamilton theorem [11] in a homogeneous flow. The coefficients of various nonlinear terms were determined from Schwarz's inequality and realizability constraints. To resolve the near-wall anisotropy, the nonlinear terms were modified by introducing additional coefficients of the strain variables. Their nonlinear model was successfully validated by predicting several turbulent flows, e.g. channel flows, flows around a backward-facing step and impinging jet. Therefore, it is expected that the aforestated features of wavy channel flow can well be predicted by employing this model.

In the preliminary stage of the present study, however, the nonlinear k–ε–f_μ model of Park et al. [9] was found to work better for predicting turbulent flows and heat transfer in a wavy channel if it is slightly modified. Emphasis is placed in the modification on the strain damping function ($f_{\mu2}$) and the wall corrections of the nonlinear terms. The model validation is therefore performed again by comparing the calculated turbulence quantities with the corresponding DNS data [12] for a fully developed flat plate channel flow. Also, for a wavy

channel flow, the model validation is made by comparing the present results with the DNS data of Maaß and Schumann [4] (obtained from ERCOFTAC database, http://ercoftac.mech.surrey.ac.uk). Turbulent flow in a channel having the undulated wall shows different behavior depending on the Reynolds number (Re_b) and wave amplitude (a). When sinusoidal undulation is applied to the wall with heat transfer, a kind of dissimilarity may exist between the momentum and heat transport. Therefore, several cases of different wave amplitude for wall undulation are studied at the Reynolds number $Re_b = 6760$ and the wavelength $\lambda = H$.

2. Turbulence models

2.1. Flow field equations

For an incompressible turbulent flow, the governing equations can be written in Cartesian tensor notation as

$$\frac{\partial U_i}{\partial x_i} = 0, \tag{1}$$

$$\frac{\partial U_i}{\partial t} + U_j \frac{\partial U_i}{\partial x_j} = -\frac{1}{\rho}\frac{\partial P}{\partial x_i} + \frac{\partial}{\partial x_j}\left[\nu \frac{\partial U_i}{\partial x_j} - \overline{u_i u_j}\right] + F_1 \delta_{1i}. \tag{2}$$

For a fully developed channel flow, the flow is driven by the forcing term F_1 (mean pressure gradient). There are two methods of providing the forcing term: one is fixing the mean pressure gradient in time or in the iteration, and the other is fixing the mass flow rate in time. In order to investigate the undulation effects, it is desirable to keep the Reynolds number based on the bulk mean velocity constant. Therefore, the latter case is adopted in the present study. The mean pressure gradient is obtained at each time step by integrating the Navier–Stokes equation in the streamwise direction [13].

2.2. Turbulence equations

The starting point of the present study is the nonlinear k–ε–f_μ model of Park et al. [9]. The basic formulation is briefly summarized below. Further details regarding the formulation can be found in Park et al. [9]. The Reynolds stress can be expressed in a conventional form as

$$-\overline{u_i u_j}^{\text{linear}} = \nu_t\left(\frac{\partial U_i}{\partial x_j} + \frac{\partial U_j}{\partial x_i}\right) - \frac{2}{3}k\delta_{ij}, \tag{3}$$

$$\begin{aligned} -\overline{u_i u_j} = {} & -\overline{u_i u_j}^{\text{linear}} - k\beta_2\left(S^*_{ik}S^*_{kj} - \frac{1}{3}S^{*2}\delta_{ij}\right) \\ & - k\beta_3(W^*_{ik}S^*_{kj} - S^*_{ik}W^*_{kj}) - k\beta_4(S^*_{il}S^*_{lm}W^*_{mj} \\ & - W^*_{il}S^*_{lm}S^*_{mj}) - k\beta_5\left(W^*_{il}W^*_{lm}S^*_{mj} + S^*_{il}W^*_{lm}W^*_{mj}\right. \\ & \left. + 0.5S^*_{ij}W^{*^2} - \frac{2}{3}III_S\delta_{ij}\right), \end{aligned} \tag{4}$$

$$\nu_t = C_\mu f_\mu \frac{k^2}{\varepsilon}, \tag{5}$$

where $\beta_2 = \tilde{\beta}_2 + \tilde{\beta}_{2,\text{wall}}C_w$, $\beta_3 = \tilde{\beta}_3 + \tilde{\beta}_{3,\text{wall}}C_w$, $\beta_4 = \tilde{\beta}_4$, $\beta_5 = \tilde{\beta}_5$, $III_S = S^*_{lm}W^*_{mn}W^*_{nl}$, $S^*_{ij} = S_{ij}k/\varepsilon$, $W^*_{ij} = W_{ij}k/\varepsilon$, $S^* = \sqrt{2S^*_{ij}S^*_{ij}}$ and $W^* = \sqrt{2W^*_{ij}W^*_{ij}}$. In the above, β_i represents the strain dependent coefficients and the model constant is set as $C_w = 1$ for $i = j$ and $C_w = 0$ for $i \neq j$.

The variations of the eddy viscosity are allowed by decomposing f_μ into two parts, i.e., $f_\mu = f_{\mu 1}f_{\mu 2}$, where $f_{\mu 1}$ signifies the effect of wall-proximity in the near-wall region while $f_{\mu 2}$ represents the strain effects [14].

$$f_{\mu 1} = (1 + f_D R_t^{-3/4})f_w^2, \tag{6}$$

$$\frac{\partial^2 f_w}{\partial x_j \partial x_j} = \frac{R_t^{3/2}}{A^2 L^2}(f_w - 1), \tag{7}$$

$$f_{\mu 2} = \frac{15}{3}\frac{1+g}{g^2 + C_\mu g^3 + A_s}, \tag{8}$$

$$g = \begin{cases} \frac{C_0}{3} + (P_1 + \sqrt{P_2})^{1/3} + \text{sign}(P_1 - \sqrt{P_2})|P_1 - \sqrt{P_2}|^{1/3}, & P_2 \geqslant 0, \\ \frac{C_0}{3} + 2(P_1^2 - P_2)^{1/6}\cos\left(\frac{1}{3}\arccos\left(\frac{P_1}{\sqrt{P_1^2 - P_2}}\right)\right), & P_2 < 0. \end{cases} \tag{9}$$

Here, the f_D function is defined as $f_D = 10\exp[-(R_t/120)^2]$ and L is a turbulence length scale $L^2 = k^3/\varepsilon^2 + 70^2\sqrt{\nu^3/\varepsilon}$ [15]. The model constants are set as $C_\mu = 0.09$ and $A = 8.4$. P_1 and P_2 are defined as

$$\begin{aligned} P_1 &= C_0\left[\frac{C_0^2}{27} - \frac{(A_s + \alpha_1\eta^2)}{6} + \frac{1}{2}\right], \\ P_2 &= P_1^2 - \left[\frac{C_0^2}{9} - \frac{(A_s + \alpha_1\eta^2)}{3}\right], \end{aligned} \tag{10}$$

where $A_s = \alpha_3^2\xi^2 - \alpha_2^2\eta^2/3$, $\alpha_1 = -0.48$ and $C_0 = 2.5$. In order to consider the wall-proximity effect in the vicinity of the wall, the mean strain rates are modified as $\eta = f_w S^*$ and $\xi = f_w W^*$.

The turbulent kinetic energy equation and its dissipation rate equation are

$$\frac{\partial k}{\partial t} + U_j\frac{\partial k}{\partial x_j} = \frac{\partial}{\partial x_j}\left[\left(\nu + \frac{\nu_t}{\sigma_k}\right)\frac{\partial k}{\partial x_j}\right] + P_k - \varepsilon, \tag{11}$$

$$\begin{aligned} \frac{\partial \varepsilon}{\partial t} + U_j\frac{\partial \varepsilon}{\partial x_j} = {} & \frac{\partial}{\partial x_j}\left[\left(\nu + \frac{\nu_t}{\sigma_\varepsilon}\right)\frac{\partial \varepsilon}{\partial x_j}\right] + \left(C^*_{\varepsilon 1}P_k - C_{\varepsilon 2}f_2\varepsilon\right)/T \\ & + C_{\varepsilon 3}(1 - f_w)\nu\nu_t\left(\frac{\partial^2 U_i}{\partial x_j \partial x_k}\right)^2, \end{aligned} \tag{12}$$

where the model constants are set as $\sigma_k = 1.1$, $\sigma_\varepsilon = 1.3$, $C_{\varepsilon 2} = 1.9$ and $C_{\varepsilon 3} = 0.8$, respectively. The model function f_2 is expressed as $f_2 = 1 - (2/9)\exp(-0.33R_t^{1/2})$, which describes the effect of decaying turbulence [16].

The turbulent timescale is defined as $T = \sqrt{(k/\varepsilon)^2 + 36(\nu/\varepsilon)}$ [15]. The strain effect is incorporated in $C^*_{\varepsilon 1}$ which has the form $C^*_{\varepsilon 1} = 1.42 + C_\mu/(1 + 5f_{\mu 2}\eta^2)$.

2.3. Modification of model coefficients

As seen in Eq. (4), $\overline{u_i u_j}$ of Park et al. [9] has the limitation that the wall corrections are restricted to the normal Reynolds stresses. In the present study, this imperfection is removed by giving modification to β_i in a way similar to the study of Park et al. [9]. Also, the strain damping function $f_{\mu 2}$ is readjusted because $f_{\mu 2}$ is connected to β_1 as $f_{\mu 2} = -\beta_1/C_\mu$. In the previous derivation without wall corrections, the model coefficients were set as $\beta_2 = 2\alpha_2\beta_1$, $\beta_3 = -\alpha_3\beta_1$, $\beta_4 = -6\alpha_2\alpha_3$ and $\beta_5 = 2\alpha_3^2\beta_1$, respectively.

In the near-wall region, the shear flow is nearly parallel except around a separation or stagnation point. In this situation, the near-wall behavior of the normal Reynolds stress is controlled by β_2 and β_3 [9]. Therefore, the special treatment is needed for β_2 and β_3. The strain dependent coefficients are now modeled as

$$\beta_2 = 4\alpha_2 C_\mu f_{\mu 2} f_w^2/g + \beta_{2,\text{wall}}, \quad \beta_3 = 2\alpha_3 C_\mu f_{\mu 2} f_w^2/g + \beta_{3,\text{wall}},$$
$$\beta_4 = -6\alpha_2\alpha_3 C_\mu f_{\mu 2} f_w^2/g^2, \quad \beta_5 = 2\alpha_3^2 C_\mu f_{\mu 2} f_w^2/g^2, \tag{13}$$

where $\beta_{2,\text{wall}} = (1 - f_w)2.0/S_w$, $\beta_{3,\text{wall}} = (1 - f_w)(1.5/S_w - 2\alpha_3 C_\mu f_{\mu 2} f_w^2/g)$ and $f_{\mu 2} = 5.41g/(g^2 + A_s)$. Here, g is a solution of Eq. (9) and the f_w function is used as a blend of the near-wall corrections with the outer-region anisotropies. The $f_{\mu 2}$ function has been tuned in the preliminary calculations for a wavy channel and backward-facing step. The model constants α_2 and α_3 are rearranged from the evaluation of Gatski and Speziale [17], i.e., $\alpha_2 = -0.375$ and $\alpha_3 = -0.8$. To correct the wall behaviors ($y^+ \leqslant 100$), the modified strain variable S_w is introduced. In the vicinity of the wall, S_w has to maintain the relation $S_w \sim O(S^{*2})$. This is because the limiting values of b_{11} and b_{22} have a non-zero value [12]. Based on the above behavior, S_w is modeled as $S_w = (1 + [\text{MAX}(S^*, W^*)]^2)/(1 + f_w)$.

In the present study, the model performance is explored by comparing the predicted results with those by the standard k–ε model and the linear k–ε–f_μ model. The model functions and model constants are summarized as follows.

For standard k–ε:

$$C_\mu = 0.09, \quad C^*_{\varepsilon 1} = 1.44, \quad C_{\varepsilon 2} = 1.92, \quad C_{\varepsilon 3} = 0.0,$$
$$\sigma_k = 1.0,$$
$$\sigma_\varepsilon = 1.3, \quad f_\mu = 1, \quad f_2 = 1, \quad T = k/\varepsilon. \tag{14}$$

For linear k–ε–f_μ:

$$C_\mu = 0.09, \quad C^*_{\varepsilon 1} = 1.42 + C_\mu/(1 + 5f_{\mu 2}\eta^2),$$
$$C_{\varepsilon 2} = 1.9, \quad C_{\varepsilon 3} = 0.8,$$
$$\sigma_k = 1.1, \quad \sigma_\varepsilon = 1.3, \quad f_\mu = f_{\mu 1} f_{\mu 2},$$
$$f_{\mu 1} = (1 + f_D R_t^{-3/4}) f_w^2, \quad f_{\mu 2} = 5.41g/(g^2 + A_s),$$
$$f_2 = 1 - (2/9)\exp(-0.33R_t^{1/2}), \quad T = \sqrt{(k/\varepsilon)^2 + 36(\nu/\varepsilon)}. \tag{15}$$

The stress–strain relationship of the above two models is obtained from $\overline{u_i u_j}^{\text{linear}}$. On the other hand, nonlinear k–ε–f_μ model has the nonlinear stress–strain relation which is expressed by the cubic relations in mean velocity gradients (see Eq. (4)). The coefficients of various nonlinear terms are determined from Eq. (13).

2.4. Model validation

It is essential to check the reliability of the present modification. Toward this end, the present model has been tested in a homogeneous shear flow and a fully developed flow between two flat plates. For a simple shear flow ($W^* = S^*$ and $f_w = 1$), the present modification is validated by showing the anisotropy prediction. The model of Craft et al. [18] is also tested for comparison. As shown in Fig. 1, the calculated normal stress anisotropies are in good agreement with the experimental [19] and DNS data [20]. The model of Craft et al. [18] shows an increasing behavior in highly strained regions ($S^* \geqslant 30$). This is attributed to the fact that the quadratic terms of their nonlinear model increase with an increase of $\sqrt{S^*}$. However, the present model satisfies the realizability limitation well. The profiles of the calculated time mean velocity and turbulent kinetic energy obtained for the flat plate channel flow are illustrated in Fig. 2 together with the DNS data [12]. Although the calculated kinetic energy is slightly overpredicted in the case of $Re_\tau = 180$, the present results show good agreement with the DNS data. The near-wall behaviors of

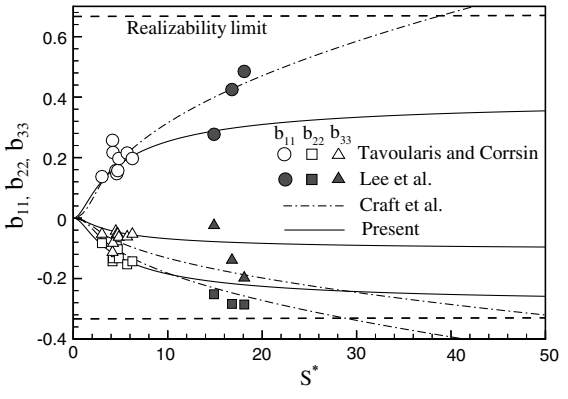

Fig. 1. Predictions of b_{11}, b_{22} and b_{33} by turbulence models.

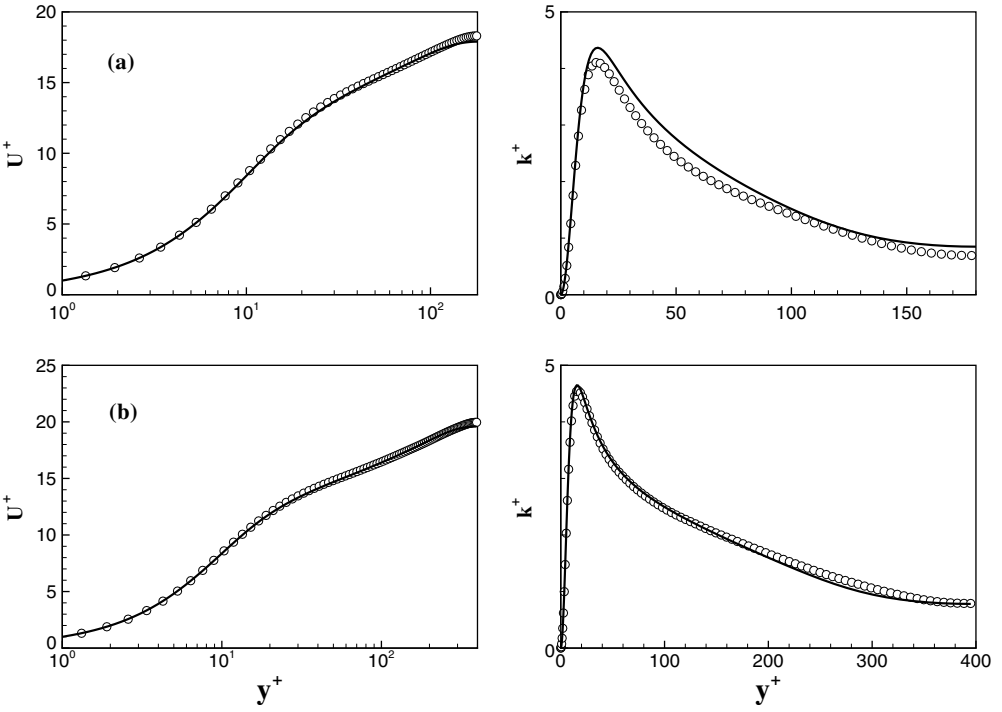

Fig. 2. Comparison of the predicted U^+ and k^+ with DNS: o, DNS [12]; —, nonlinear k–ε–f_μ. (a) $Re_\tau = 180$ and (b) $Re_\tau = 395$.

Reynolds stresses are presented in Fig. 3. The near-wall anisotropy in the region of $y^+ \leqslant 100$ is well captured with the present model and as is demonstrated in the figure the computed anisotropy is strongly affected by the two constants $\beta_{2,\mathrm{wall}}$ and $\beta_{3,\mathrm{wall}}$.

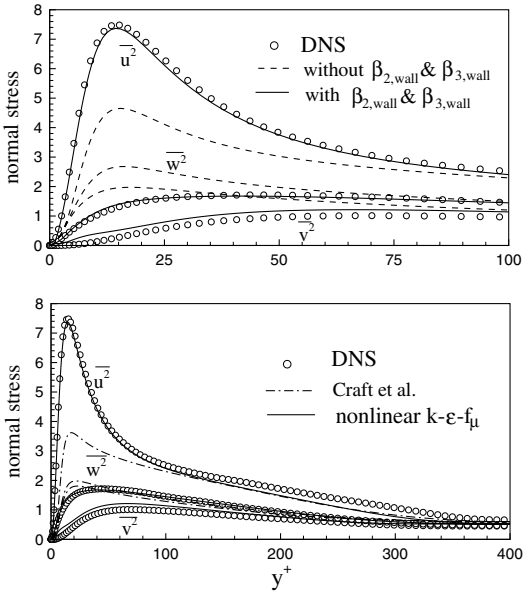

Fig. 3. Comparison of $\overline{u^2}^+$, $\overline{v^2}^+$ and $\overline{w^2}^+$ with DNS [12].

3. Thermal field equation

In calculating turbulent heat transfer, the explicit algebraic heat flux model of Park et al. [9] is adopted. The governing equation of mean temperature is expressed as

$$\frac{\partial \Theta}{\partial t} + U_j \frac{\partial \Theta}{\partial x_j} = \frac{\partial}{\partial x_j}\left[\frac{\nu}{Pr}\frac{\partial \Theta}{\partial x_j} - \overline{\theta u_j}\right]. \tag{16}$$

The Prandtl number is set as $Pr = 0.7$. The heat flux $-\overline{\theta u_j}$ is determined by

$$\overline{\theta u_i} = -\alpha_t\left(\frac{2}{3}\delta_{ij} + 2f_w b_{ij}\right)\Theta_{,j} - \alpha_{ik}\left(S^\theta_{km} + W^\theta_{km}\right)\Theta_{,m} - 2\alpha_{ik}\left(S^\theta_{kl}S^\theta_{lm} + W^\theta_{kl}W^\theta_{lm} + S^\theta_{kl}W^\theta_{lm} + W^\theta_{kl}S^\theta_{lm}\right)\Theta_{,m}, \tag{17}$$

where $\alpha_{ik} = \alpha_t\gamma_2(\overline{u_i u_k}/k)$, $S^\theta_{ij} = C_{T2}S_{ij}(k/\varepsilon)$ and $W^\theta_{ij} = C_{T3}W_{ij}(k/\varepsilon)$. In the above equation, γ_2 prevents an excessive increase of the strain dependent terms. The γ_2 function is defined by $\gamma_2 = f_w(2+\eta_t^*)/[2+\xi_s^2+\eta_t^*(1+\eta_t^*)]$, where $\eta_t^* = \xi_t^2 - \eta_t^2$, $\xi_s = \mathrm{MAX}(\xi_t^2, \eta_t^2)$, $\eta_t = \sqrt{S^\theta_{ij}S^\theta_{ij}}$ and $\xi_t = \sqrt{W^\theta_{ij}W^\theta_{ij}}$. The model constants are set as $C_{T2} = 0.2$ and $C_{T3} = 0.12$.

The thermal diffusivity is expressed as $\alpha_t = C_\lambda f_\lambda \nu_t$. The coefficient C_λ is a function of R_t and Pr [21]. The

near-wall effect of α_t is incorporated in the f_λ function. The coefficient C_λ and the f_λ function are modeled as

$$f_\lambda = [1 - \exp(-8f_w)]^3, \tag{18}$$

$$C_\lambda = \frac{2}{3}\left(1 + \frac{12.5}{R_t^{0.5}}\right)^2 \left(1 + \frac{130}{R_t Pr}\right)^{-0.25}. \tag{19}$$

4. Numerical procedure

A fractional-step method is used to solve the governing equations. The spatial discretization is performed with the fourth-order compact scheme [22] for the convective term in Eq. (2) and the HLPA scheme [23] for the convective term in k-, ε- and Θ-equation. The viscous term and the other terms are evaluated by the fourth-order central-differencing. A non-staggered grid arrangement is adopted. So, the momentum interpolation technique is employed to avoid the pressure–velocity decoupling. The time integration is based on a hybrid scheme using the third-order Runge–Kutta method for the explicitly treated terms and the Crank–Nicolson method for the implicitly treated terms. The implicit terms in each equation are the diffusion terms without cross derivatives. The explicit terms are the diffusion terms with cross derivatives and the source terms. Details regarding this hybrid scheme can be found in You et al. [13]. Convergence of Poisson equation for pressure is accelerated with a multigrid method [24]. The computation was judged to have converged when the normalized sum of absolute residual sources over all the computational nodes has come down to a value less than 10^{-4}.

Fig. 4 shows the computational domain for a wavy wall channel. The streamwise and vertical coordinates are denoted by x and y. Periodic boundary conditions are applied at upstream and downstream ends of the computational domain. In the y direction, the lower wall has the undulation of sinusoidal shape of the amplitude a and its mean position is located at $y = 0$. The upper flat wall is located at $y = H$. The location of the wavy wall, y_w, is given by $y_w = a\cos(2\pi x/\lambda)$. The wall boundary conditions employed are: $U = V = k = f_w = 0$, $\varepsilon_w = 2\nu k/n_{first}^2$, and $\partial P/\partial n = 0$, where n_{first} is the wall-normal distance between the wall surface and the first grid point, and n implies the normal direction against the wall surface. The flat wall is maintained at a constant temperature Θ_C while the wavy wall is heated at another constant temperature Θ_H. The maximum value of $n^+ \equiv u_\tau n/\nu$ at the first grid point is $n^+_{max} = 0.5$.

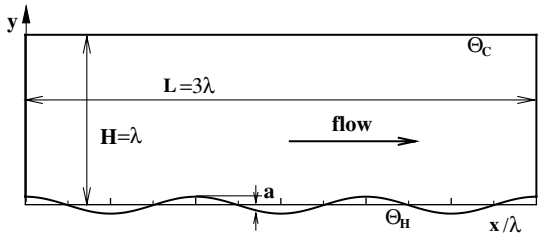

Fig. 4. Computational domain of flow over a wavy wall.

5. Results and discussion

Turbulent flow past a wavy wall channel can be categorized into several regimes depending on the Reynolds number and wall wave amplitude. It is expected that a linear response is observed for the case of small amplitude and at low Reynolds numbers. As both increase, a nonlinear response is observed and a separated flow appears. The boundaries between these regimes are still obscure. Therefore, it is desirable to analyze the response of flow characteristics to the wall wave amplitudes. The wall wave amplitude is varied in the range $0 \leqslant a/\lambda \leqslant 0.15$. The Reynolds number is fixed at $Re_b = 6760$ for all wave amplitudes, corresponding to the value adopted in the DNS of Maaß and Schumann [4]. The grid dependency was checked by carrying out the computation for the four cases: 92×82, 122×102, 152×102 and 152×122. In all the cases, the value of Courant–Friedrichs–Lewy number was kept smaller than unity. Flow Reynolds number is $Re_b = 6760$ as described above and wall undulation amplitude is $a/\lambda = 0.05$ where a is the undulation amplitude and λ the wavelength. As shown in Fig. 5, the result with a 122×102 mesh was found to be satisfactory.

Now the applicability of the presently modified nonlinear k–ε–f_μ model is further discussed by comparing the present results with those obtained with the standard k–ε model, the linear k–ε–f_μ model and the low Reynolds number k–ε model by Abe et al. [25] (hereafter called AKN model), which is popularly included in the

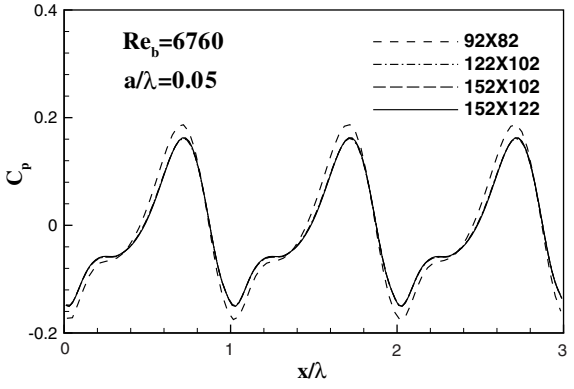

Fig. 5. Grid convergence test.

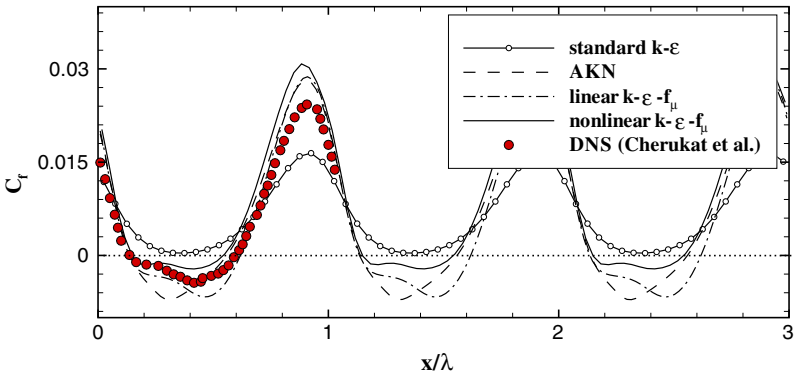

Fig. 6. Comparison of the predicted C_f ($\lambda = H$ and $a = 0.05H$): o, DNS by Maaß and Schumann [4]; –o–, standard k–ε; ----, AKN by Abe et al. [25]; -·-, linear k–ε–f_μ; —, nonlinear k–ε–f_μ.

test of turbulence models. Fig. 6 shows the streamwise distribution of the wall friction coefficient C_f along the undulant wall. The value of C_f reflects the alternating appearance of the favorable and adverse pressure gradient or the appearance of flow separation and reattachment in the case of a deep undulation. As can be seen in the figure, the standard k–ε model cannot predict the appearance of flow separation which should actually appear at this wall wave amplitude. This indicates that the wall function treatment does no longer work in this case. In addition, the standard k–ε model responds only obtusely to the flow acceleration resulting in a lower peak of C_f. On the other hand, the appearance of flow separation can be predicted with the nonlinear k–ε–f_μ model. The linear k–ε–f_μ model also works quite well in this sense. AKN model gives reasonable results in a point that the obtained value of C_f becomes negative in the trough of the wall undulation. However, it is not very good in another sense. Its distribution profile does not have such two local minima as the results of DNS have. So, the present nonlinear k–ε–f_μ model works slightly better in this point.

The separation (x_s) and reattachment (x_r) points are predicted as $x_s = 0.135\lambda$ and $x_r = 0.61\lambda$ for linear k–ε–f_μ model. Here, x_s and x_r are defined as locations where wall shear stress vanishes. Comparing with the prediction of linear k–ε–f_μ model, the nonlinear model predicts a short recirculation zone, i.e., $x_s = 0.14\lambda$ and $x_r = 0.57\lambda$. Table 1 tabulates the presently calculated positions of the flow separation and flow reattachment points together with the DNS data reported by Maaß and Schumann [4] and Cherukat et al. [5] and the experimental data by Hudson [2]. The present results agree well with the DNS data.

Table 1
Comparison of x_s and x_r ($Re_b = 6760$, $\lambda = H$ and $a = 0.05H$)

Case	Separation (x_s)	Reattachment (x_r)
Hudson	0.22λ	0.58λ
Maaß and Schumann	0.15λ	0.59λ
Cherukat et al.	0.14λ	0.59λ
AKN	0.14λ	0.56λ
Linear k–ε–f_μ	0.135λ	0.61λ
Nonlinear k–ε–f_μ	0.140λ	0.57λ

The results obtained with the three models are now discussed in terms of the time mean velocity components and turbulence quantities. Fig. 7 shows the transverse distributions of the streamwise and transverse components of time mean velocity U/U_b and V/U_b at four different streamwise locations. The predicted results with the three turbulence models are compared with the DNS data of Maaß and Schumann [4]. The U/U_b profile shows the asymmetry caused by the difference of the surface drag between the two wall boundaries. The linear k–ε–f_μ model and the present nonlinear k–ε–f_μ model give almost the same results for the U/U_b profile. However, they work differently in the prediction of V/U_b profile and the nonlinear k–ε–f_μ model works slightly better near the wall. This implies that the nonlinear stress–strain relation has a significant effect in the wavy side near-wall region, where the strain and rotation rates are very strong. These effects are appropriately included in the nonlinear stress–strain relation in conjunction with the elliptic f_w equation. On the contrary, all the predictions with the three models show a good agreement near the wave crest ($x/\lambda = 0.992$). Fig. 8 shows the distributions of Reynolds stresses together with the counterparts of DNS. The normal stresses of the standard k–ε model and the linear k–ε–f_μ model are obtained by making use of the relationship $\overline{u_i u_j} = 2k\delta_{ij}/3 - 2\nu_t S_{ij}$. As can be seen in Fig. 8, the predicted results of $\overline{u^2}/U_b^2$ and $\overline{v^2}/U_b^2$ are underpredicted with any of the models if compared with the DNS data. However, the nonlinear k–ε–f_μ model is found to give better results for the turbulence quantities among them. The present results of the Reynolds normal stress $\overline{u^2}/U_b^2$ and the Reynolds shear stress $-\overline{uv}/U_b^2$ obtained with the

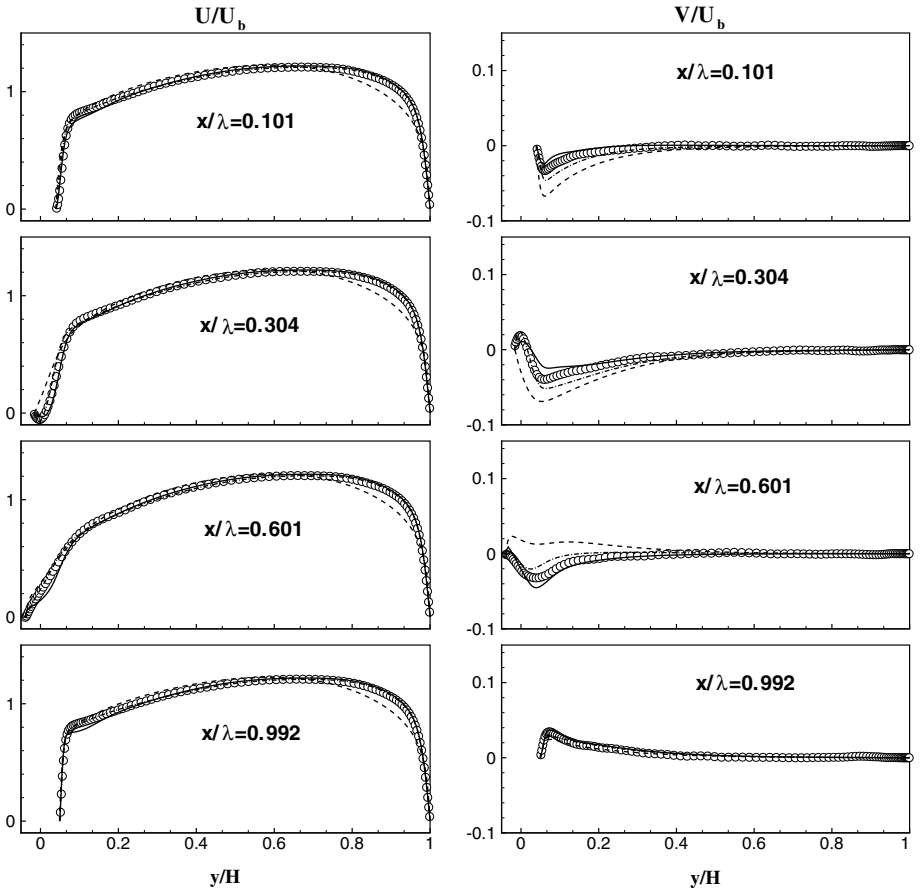

Fig. 7. Comparison of U/U_b and V/U_b with DNS: o, Maaß and Schumann [4]; ----, standard k–ε; -·-, linear k–ε–f_μ; —, nonlinear k–ε–f_μ.

nonlinear k–ε–f_μ model agree quite well with the DNS data, while the value of $\overline{v^2}/U_b^2$ is a little overpredicted at the wavy wall side. All these points indicate that the nonlinear stress–strain relationship introduced in the nonlinear k–ε–f_μ model is effective to simulate the nonlinear flow behavior near the wavy wall of the channel.

The effects of wall undulation on the flow and heat transfer are now addressed in a little more detail based on the results obtained with the nonlinear k–ε–f_μ model. The comprehensive examination of wall friction is prerequisite because the convective heat transfer is closely linked to the flow structure in the near-wall region. The evolution of the local skin friction coefficient (C_f) and streamlines computed by the nonlinear k–ε–f_μ model at various wave amplitudes (a/λ) are plotted in Fig. 9. All of the C_f profiles have similar general features; i.e., the peaks of skin friction occur near the wavy crest and there is a minimum friction in the wavy trough. For $a/\lambda = 0.01$, the flow boundary layer still exists on the wavy wall and produces the sinusoidal change of C_f. To make this clearer, the predicted streamlines are compared in the figure. For $a/\lambda = 0.03$, a small separation zone is detected in the trough of the wavy wall. As a/λ further increases, the flow separation and reattachment become more noticeable. This recirculating flow causes the deviation from the sinusoidal variation of the local C_f. However, its periodic spatial distribution in the trough region is not seriously changed by the variation of the wall wave amplitude. To make the effects of the wall undulation clearer, attention is now turned to the spatial mean quantities. The predicted total C_D, flow separation point x_s and flow reattachment point x_r at various wall wave amplitudes are plotted in Fig. 10. The total mean drag coefficient is calculated integrating the forces acting on the wall surface: $C_D = C_{D\tau} + C_{Dp} = (1/A)\int \tau_{wall} S_y \, dA + (1/A)\int P_{wall} S_x \, dA$, where A is the area of wall surface, S_x and S_y are x- and y-components of unit normal vector against the wall surface. $C_{D\tau}$ and C_{Dp} are the friction drag and the form drag normalized by $\rho U_b^2/2$. As seen in the distributions of x_s and x_r, it is interesting to find that the growth of separation zone is initiated at $a/\lambda \sim 0.02$. For $a/\lambda \geqslant 0.02$, the mean drag

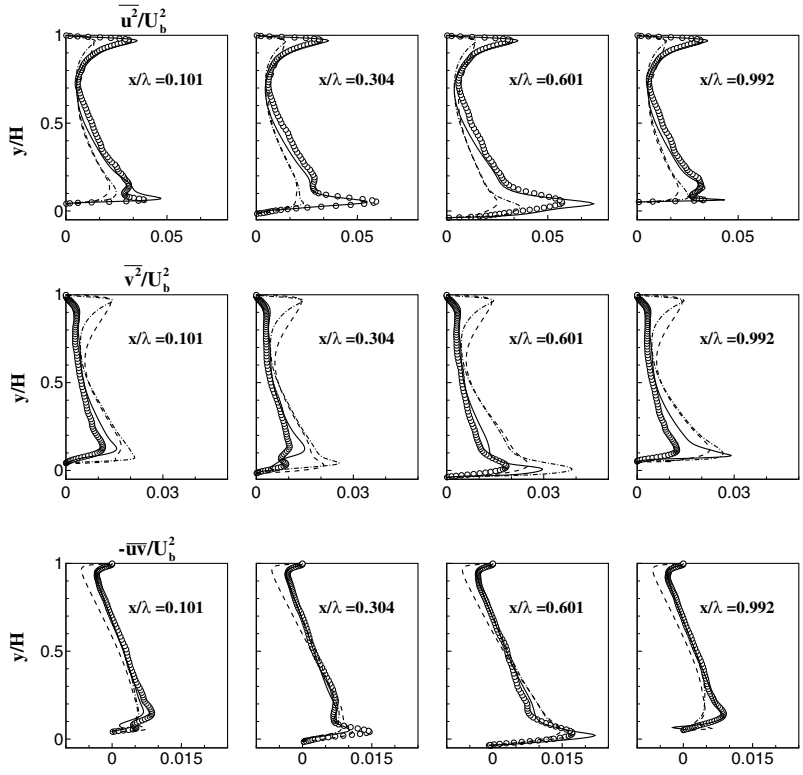

Fig. 8. Comparison of $\overline{u^2}/U_b^2$, $\overline{v^2}/U_b^2$ and $-\overline{uv}/U_b^2$ with DNS: symbol and line patterns as in Fig. 7.

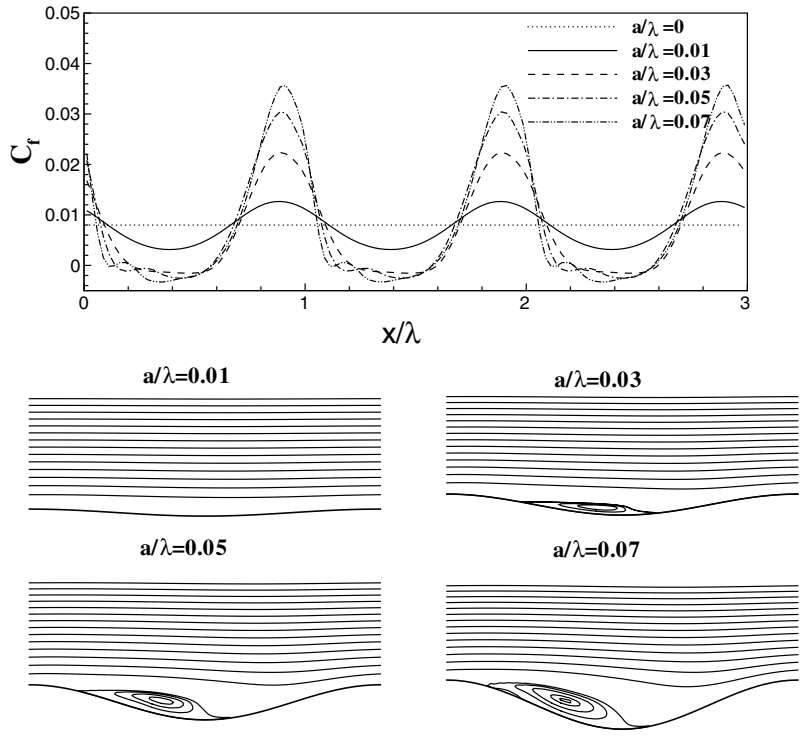

Fig. 9. Comparison of the predicted C_f and streamlines.

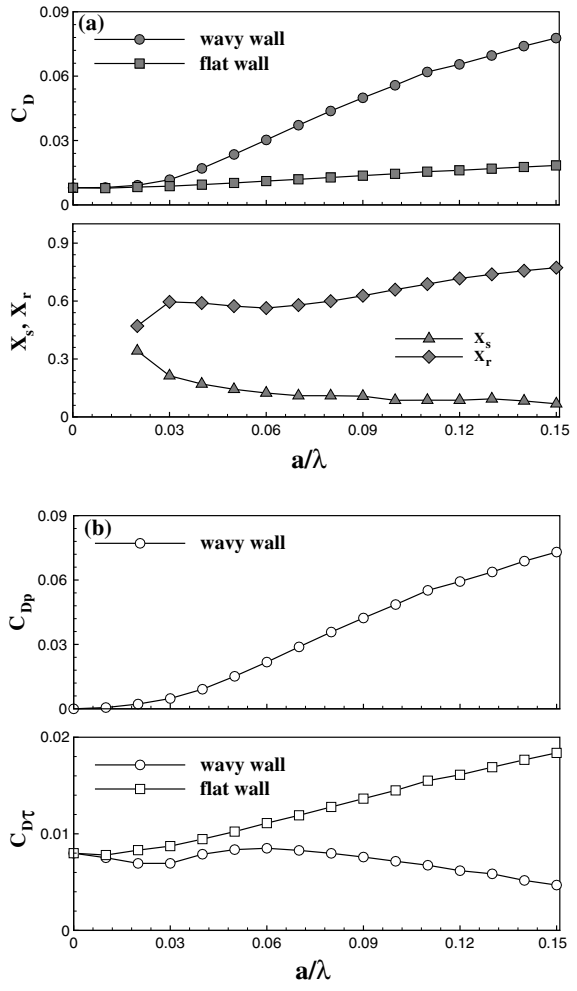

Fig. 10. Comparison of the predicted C_D, x_s and x_r: (a) total drag and separation/reattachment point and (b) form drag and friction drag.

C_D is significantly increased in the wavy wall because of the increase of the blockage effect. Undulation of one wall exerts a non-negligible effect on the friction drag on the another wall. To separate the contributions of wall friction and wall pressure in the mean drag, C_D is decomposed into the form drag and friction drag. As a/λ increases, the form drag shows a monotonic increase and the friction drag becomes to be overwhelmed by the form drag. For example, at $a/\lambda = 0.15$ the form drag is 15.5 times larger than the friction drag. This increasing trend of form drag with an increase of the wall wave amplitude can also be seen in Henn's work [26]. On the other hand, the friction drag $C_{D\tau}$ takes maximum value at $a/\lambda \sim 0.06$. This is important since it is closely related to the development of the recirculating flow region in the wavy wall trough. A closer inspection of x_s and x_r indicates that as the wave wall amplitude is further increased in the range $a/\lambda \geqslant 0.06$, the separated flow region is enlarged with an increase of a/λ. The friction drag then decreases gradually and at $a/\lambda = 0.15$, it is reduced to 58.8% of that of the flat channel.

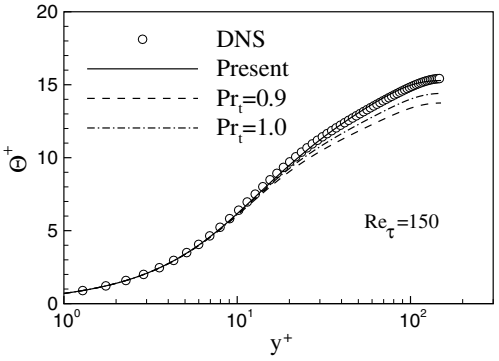

Fig. 11. Comparison of the predicted Θ^+ with DNS [27].

In order to investigate the undulation effects for heat transfer, several simulations are performed at various magnitudes of wall wave amplitude. Discussion will be given firstly to the test of the present heat flux model because the coefficients of nonlinear stress–strain relation in the nonlinear k–ε–f_μ model have slightly been changed. Fig. 11 shows the predicted mean temperature profile for a fully developed turbulent flow in a flat plate channel by using Eq. (17). A good agreement with the DNS data [27] is found for the mean temperature. In contrast to this, the results obtained with constant Pr_t assumptions ($\overline{\theta u_i} = -(\nu_t/Pr_t)\partial\Theta/\partial x_i$) slightly underpredict the mean temperature. The effect of the wall wave amplitudes on Nu is examined in Fig. 12. As shown in Fig. 12(a)–(b), nine cases are selected to demonstrate the effect of wall undulation on the wall heat transfer. As a/λ increases, the deviation from the sinusoidal variation is magnified in the spatial distribution of Nu. For large-amplitude wall waves, the local variation of Nu is affected by the appearance of flow separation. However, the peaks of the local Nu occur near the wavy crest, where the inviscid free-stream velocity is maximum. To see the overall influence of wall wave amplitude on the wall heat transfer, the mean Nusselt number is displayed in Fig. 12(c). The mean Nu is calculated by $Nu_{\text{avg}} = \int Nu\,\mathrm{d}A/A$. The present heat flux model is compared with the results obtained employing the constant Pr_t assumption ($Pr_t = 0.9$). Even though the predicted values are very different, two predictions show a common behavior of wall heat transfer. As the wall wave amplitude increases from $a/\lambda = 0$ to $a/\lambda = 0.15$, the maximum heat transfer rate is obtained at $a/\lambda \geqslant 0.11$. This is somehow similar to a feature that $C_{D\tau}$ takes maximum value at $a/\lambda \sim 0.06$. As can be seen in Fig. 12(a)–(b), the lowest Nu for $a/\lambda \geqslant 0.06$ is larger than that of the flat case ($a/\lambda = 0$) and the Nu distribution gradually loses

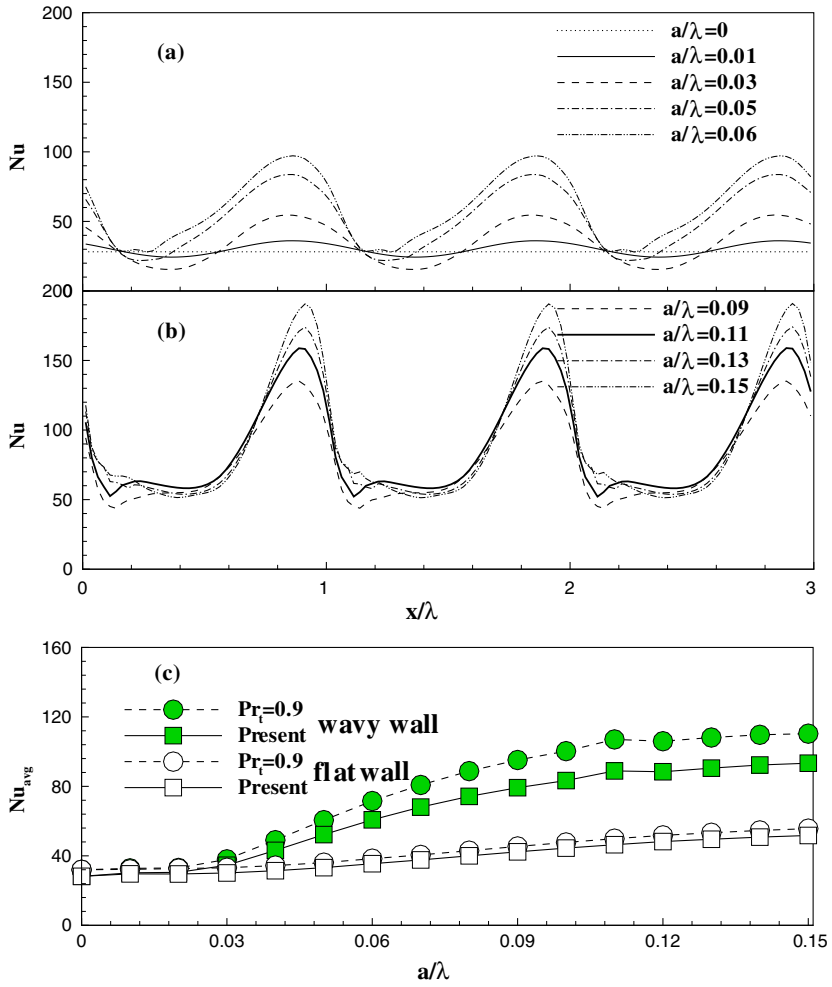

Fig. 12. Comparison of the predicted *Nu*.

sinusoidal feature as a/λ increases. Moreover, the lower-valued region of *Nu*, the region where the local *Nu* is less than Nu_{avg}, is enlarged. This trend reflects the special interrelation between the decrease of *Nu* in the recirculating flow region and the increase of *Nu* near the wavy crest. Therefore, a closer inspection of Figs. 10 and 12 indicates that the variation of the mean *Nu* is characterized by the change of the size of recirculating flow region. The maximum heat transfer rate is closely related to the strength of the reversal flow in the wavy trough.

To scrutinize the turbulence structure in wavy wall channel, the distributions of production of turbulent kinetic energy (hereafter abbreviated as turbulent production, P_k), production rate of temperature fluctuation intensity (hereafter abbreviated as turbulent thermal production, $P_\theta = -\overline{u_j\theta}\partial\Theta/\partial x_j$) and turbulent heat flux ($\overline{v\theta}$) are displayed in Fig. 13. Each variable is normalized by the friction velocity u_τ and the friction temperature θ_τ which are both averaged on wall surfaces. The representative two cases are selected; the non-separated regime of $a/\lambda = 0.01$ and the separated regime of $a/\lambda = 0.07$. u_τ and θ_τ are predicted as: $u_\tau = 212.9\nu$ and $\theta_\tau = 0.0251$ for $a/\lambda = 0.01$; $u_\tau = 239.8\nu$ and $\theta_\tau = 0.0379$ for $a/\lambda = 0.07$. As seen in Fig. 13, the turbulent thermal production is closely correlated to the changes of $\overline{v\theta}$ and P_k. For $a/\lambda = 0.01$, the variations of P_k and P_θ are restricted to the region near the wall. The effect induced by the wavy wall is confined near the wavy crest. For this wall wave amplitude, variation of the flow and heat transfer with wall undulation is linear, because the disturbance by the wall undulation is not large. Variations of the flow and heat transfer characteristics are more pronounced for $a/\lambda = 0.07$. In the recirculation region, the turbulent production and turbulent thermal production are increased because of the nonlinear strains

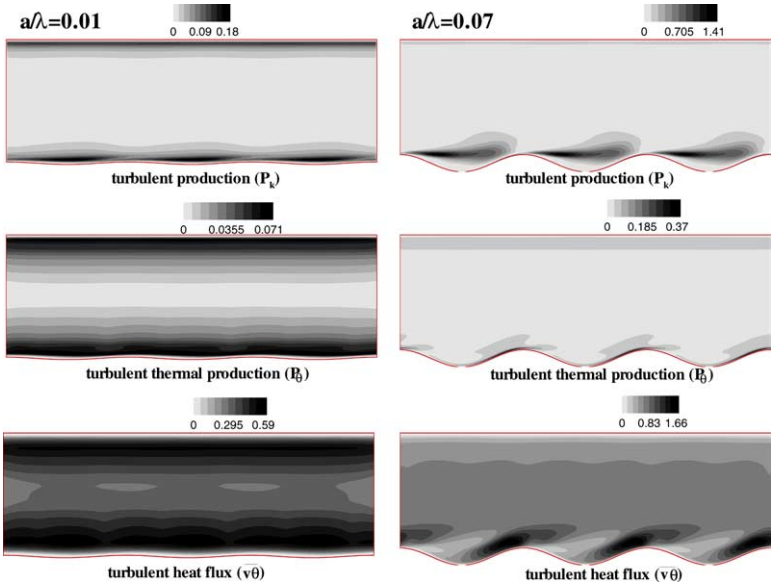

Fig. 13. Variation of P_k, P_θ and $\overline{v\theta}$ with the change in the amplitude of the wall waviness.

produced in the separated shear layer. However, the turbulent thermal production is reduced in the wavy trough. This may be caused by the fact that temperature gradient is reduced as a result of the intensified mixing of the fluid in the recirculating flow region. Downstream the reattachment point, the heated flow is convected to the wavy crest under the favorable pressure gradient. This flow acceleration gives rise to the enhancement of the turbulent production and turbulent thermal production near the wavy crest.

6. Conclusions

The nonlinear k–ε–f_μ model of Park et al. [9] has been modified and applied for the prediction of turbulent flows and heat transfer in a wavy wall channel. The wall corrections of the nonlinear terms were made through the model coefficients related to the modified strain variable (S_w). For a fully developed flat plate channel flow, the present modification was validated by comparing the calculated turbulence quantities with the DNS data [12,27]. For the wavy channel ($a = 0.05H$), the model validation was made by comparing with the DNS data of Maaß and Schumann [4]. The predicted results were in generally good agreement with the DNS data. In order to analyze the effect of surface undulation, several wall wave amplitudes in the range $0 \leqslant a/\lambda \leqslant 0.15$ were selected for $Re_b = 6760$ and $\lambda = H$. The results showed that the local variations of the wall friction and the heat transfer rate were altered by the degree of surface undulation. It was found that the separated flow is initiated almost at $a/\lambda = 0.02$. As a/λ is increased, the size of the flow recirculation zone was slightly enlarged. Although the distributions of C_f and Nu were affected by the appearance of the flow recirculation zone, their patterns are similar with the shape of wavy wall surface. For the wavy wall surface, the drag coefficient and the heat transfer rate were higher than that of the flat wall related to the appearance of the flow recirculation zone. As the wave amplitude was increased from $a/\lambda = 0$ to $a/\lambda = 0.15$, the overall C_D showed a unilateral increment because of the increased form drag. However, the friction drag was significantly reduced and the highest heat transfer rate is observed at $a/\lambda \geqslant 0.11$. The effects of the wall wave amplitude on the flow and heat transfer characteristics were well captured by combining the modified nonlinear k–ε–f_μ model with the explicit algebraic heat flux model of Park et al. [9].

References

[1] J. Buckles, T.J. Hanratty, R.J. Adrian, Turbulent flow over a large-amplitude wavy surface, J. Fluid. Mech. 140 (1984) 27–44.
[2] J.D. Hudson, The effect of a wavy boundary on turbulent flow, Ph.D. thesis, University of Illinois, Urbana, IL, 1993.
[3] J.D. Hudson, L. Dykhno, T.J. Hanratty, Turbulence production in flow over a wavy wall, Exp. Fluids 20 (1996) 257–265.
[4] C. Maaß, U. Schumann, Direct numerical simulation of separated turbulent flow over a wavy boundary. In: E.H.

Hirschel (Ed.), Flow simulation with high performance computers, Notes on numerical fluid mechanics 52 (1996) 227–241.
[5] P. Cherukat, Y. Na, T.J. Hanratty, J.B. Mclaughlin, Direct numerical simulation of a fully developed turbulent flow over a wavy wall, Theoret. Comp. Fluid Dyn. 11 (1998) 109–134.
[6] K. Matsubara, T. Miyamae, H. Suto, M. Kobayashi, DNS study of turbulent flow and heat transfer over wavy surfaces, In: J. Taine (Ed.), Proceedings of the Twelfth International Heat Transfer Conference, 2002, pp. 195–200.
[7] J.W. McLean, Computation of turbulent flow over a moving wavy boundary, Phys. Fluids 26 (1983) 2065.
[8] V.V. Patel, J. Tyndall Chon, J.Y. Yoon, Turbulent flow in a channel with a wavy wall, ASME J. Fluid Eng. 113 (1991) 579–586.
[9] T.S. Park, H.J. Sung, K. Suzuki, Development of a nonlinear near-wall turbulence model for turbulent flow and heat transfer, Int. J. Heat Fluid Flow 24 (2003) 29–40.
[10] T.S. Park, H.J. Sung, A new low-Reynolds-number k–ε–f_μ model for predictions involving multiple surfaces, Fluid Dyn. Res. 20 (1997) 97–113.
[11] S.B. Pope, A more effective-viscosity hypothesis, J. Fluid Mech. 72 (1975) 331–340.
[12] R.D. Moser, J. Kim, N.N. Mansour, Direct numerical simulation of turbulent channel flow up to $Re_\tau = 590$, Phys. Fluids 11 (1999) 943–945.
[13] J. You, H. Choi, J.Y. Yoo, A modified fractional step method of keeping a constant mass flow rate in fully developed channel and pipe flows, KSME Int. J. 14 (2000) 547–552.
[14] T.S. Park, H.J. Sung, A nonlinear low-Reynolds-number k–ε model for turbulent separated and reattaching flows—(I) flow field computation, Int. J. Heat Mass Transfer 38 (1995) 2657–2666.
[15] P.A. Durbin, D. Laurence, Nonlocal effects in single point closure, In: Proceedings of the Third Advances in Turbulence Research Conference, Korea Univ., Korea, 1996, pp. 109–120.
[16] G.N. Coleman, N.N. Mansour, Simulation and modeling of homogeneous compressible turbulence under isotropic mean compression, selected papers from the Eighth International Symposium on Turbulent Shear Flows, Springer-Verlag, 1993, pp. 269–282.
[17] T.B. Gatski, C.G. Speziale, On explicit algebraic stress models for complex turbulent flows, J. Fluid Mech. 254 (1993) 59–78.
[18] T.J. Craft, B.E. Launder, K. Suga, Development and application of a cubic eddy-viscosity model of turbulence, Int. J. Heat Fluid Flow 17 (1996) 108–115.
[19] S. Tavoularis, S. Corrsin, Experiments in nearly homogeneous turbulent shear flow with a uniform mean temperature gradient. Part I, J. Fluid Mech. 104 (1981) 311–347.
[20] M.J. Lee, J. Kim, P. Moin, Structure of turbulence at high shear rate, J. Fluid Mech. 216 (1990) 561–583.
[21] M.M. Rogers, N.N. Mansour, W.C. Reynolds, An algebraic model for the turbulent flux of a passive scalar, J. Fluid Mech. 203 (1989) 77–101.
[22] S.K. Lele, Compact finite difference schemes with spectral-like resolution, J. Comput. Phys. 103 (1992) 16–42.
[23] J. Zhu, Higher-order bounded discretization schemes for finite volume computations of incompressible flows, Comput. Meth. Appl. Mech. Eng. 98 (1992) 345–360.
[24] T.S. Park, Multigrid method and low-Reynolds-number k–ε model for turbulent recirculating flows, Numer. Heat Transfer Part B: Fundamentals 36 (1999) 433–456.
[25] K. Abe, T. Kondoh, Y. Nagano, A new turbulence model for predicting fluid flow and heat transfer in separating and reattaching flows—1. flow field calculations, Int. J. Heat Mass Transfer 37 (1994) 139–151.
[26] D.S. Henn, R.I. Sykes, Large-eddy simulation of flow over wavy surface, J. Fluid Mech. 383 (1999) 75–112.
[27] N. Kasagi, Y. Tomita, A. Kuroda, Direct numerical simulation of passive scalar field in a turbulent channel flow, ASME J. Heat Transfer 114 (1992) 598–606.